



## OPEN ACCESS

EDITED BY  
Giulio Fracasso,  
University of Padova,  
Italy

REVIEWED BY  
Anna Lankoff,  
Institute of Nuclear Chemistry and  
Technology (INCT), Poland  
Mário Barros,  
Klinikum Chemnitz gGmbH, Germany

\*CORRESPONDENCE  
Heather M. Gibson  
✉ Gibsonh@karmanos.org

RECEIVED 30 August 2023  
ACCEPTED 08 November 2023  
PUBLISHED 07 December 2023

CITATION  
Hackett JB, Ramos N, Barr S, Bross M,  
Viola NT and Gibson HM (2023) Interferon  
gamma immunoPET imaging to evaluate  
response to immune checkpoint inhibitors.  
*Front. Oncol.* 13:1285117.  
doi: 10.3389/fonc.2023.1285117

COPYRIGHT  
© 2023 Hackett, Ramos, Barr, Bross, Viola  
and Gibson. This is an open-access article  
distributed under the terms of the [Creative  
Commons Attribution License \(CC BY\)](https://creativecommons.org/licenses/by/4.0/). The  
use, distribution or reproduction in other  
forums is permitted, provided the original  
author(s) and the copyright owner(s) are  
credited and that the original publication in  
this journal is cited, in accordance with  
accepted academic practice. No use,  
distribution or reproduction is permitted  
which does not comply with these terms.

# Interferon gamma immunoPET imaging to evaluate response to immune checkpoint inhibitors

Justin B. Hackett, Nicholas Ramos, Stephen Barr,  
Madeline Bross, Nerissa T. Viola and Heather M. Gibson\*

Karmanos Cancer Institute, Department of Oncology, Wayne State University School of Medicine,  
Detroit, MI, United States

**Introduction:** We previously developed a  $^{89}\text{Zr}$ -labeled antibody-based immuno-positron emission tomography (immunoPET) tracer targeting interferon gamma (IFN $\gamma$ ), a cytokine produced predominantly by activated T and natural killer (NK) cells during pathogen clearance, anti-tumor immunity, and various inflammatory and autoimmune conditions. The current study investigated [ $^{89}\text{Zr}$ ]Zr-DFO-anti-IFN $\gamma$  PET as a method to monitor response to immune checkpoint inhibitors (ICIs).

**Methods:** BALB/c mice bearing CT26 colorectal tumors were treated with combined ICI (anti-cytotoxic T-lymphocyte-associated protein 4 (CTLA-4) and anti-programmed death 1 (PD-1)). The [ $^{89}\text{Zr}$ ]Zr-DFO-anti-IFN $\gamma$  PET tracer, generated with antibody clone AN18, was administered on the day of the second ICI treatment, with PET imaging 72 hours later. Tumor mRNA was analyzed by quantitative reverse-transcribed PCR (qRT-PCR).

**Results:** We detected significantly higher intratumoral localization of [ $^{89}\text{Zr}$ ]Zr-DFO-anti-IFN $\gamma$  in ICI-treated mice compared to untreated controls, while uptake of an isotype control tracer remained similar between treated and untreated mice. Interestingly, [ $^{89}\text{Zr}$ ]Zr-DFO-anti-IFN $\gamma$  uptake was also elevated relative to the isotype control in untreated mice, suggesting that the IFN $\gamma$ -specific tracer might be able to detect underlying immune activity *in situ* in this immunogenic model. In an efficacy experiment, a significant inverse correlation between tracer uptake and tumor burden was also observed. Because antibodies to cytokines often exhibit neutralizing effects which might alter cellular communication within the tumor microenvironment, we also evaluated the impact of AN18 on downstream IFN $\gamma$  signaling and ICI outcomes. Tumor transcript analysis using interferon regulatory factor 1 (IRF1) expression as a readout of IFN $\gamma$  signaling suggested there may be a marginal disruption of this pathway. However, compared to a 250  $\mu\text{g}$  dose known to neutralize IFN $\gamma$ , which diminished ICI efficacy, a tracer-equivalent 50  $\mu\text{g}$  dose did not reduce ICI response rates.

**Discussion:** These results support the use of IFN $\gamma$  PET as a method to monitor immune activity *in situ* after ICI, which may also extend to additional T cell-activating immunotherapies.

## KEYWORDS

interferon gamma, immunoPET imaging, immunotherapy, immune checkpoint inhibitors, radioactive tracer

## Introduction

Modern cancer immunotherapy approaches have improved clinical outcomes for a subset of malignancies, and immune checkpoint inhibitors (ICI) are among the most promising of these modalities. Immune checkpoints are ligand:receptor interactions that regulate the activity of inflammatory cells. These checkpoints are critical for tempering immune activity; they play a major role in slowing the immune response to prevent excessive tissue damage and/or autoimmunity after a trigger, such as an infection (1–3). In cancer, immune checkpoints are coopted by malignant cells to escape immune-mediated attack. FDA-approved ICI therapies have primarily targeted two inhibitory signaling axes: cytotoxic T-lymphocyte-associated protein 4 (CTLA-4) and programmed death 1 (PD-1) with its primary ligand PD-L1. Both CTLA-4 and PD-1/PD-L1 signaling down-regulate the inflammatory effector functions of multiple immune cell subtypes, including CD8<sup>+</sup> T-cells [reviewed in (4)]. Recently, an antibody targeting lymphocyte-activation gene 3 (LAG-3) received Food and Drug Administration (FDA) approval (5) and several additional targets are undergoing clinical testing (6).

Combination of ICI therapies has proven beneficial for advanced melanoma, lung, and renal carcinomas (5, 7–13). Melanoma is recognized as the most responsive cancer to this therapy. Despite its notable clinical success, durable response to combined ICI in metastatic melanoma is less than 50%, and it remains unclear what factors differentiate which patients will benefit (5, 11–13). PD-L1 expression is an imperfect biomarker that neither precludes nor guarantees response to PD-1/PD-L1-directed therapies (reviewed in (14)). Tumor mutational burden is somewhat reliable as a biomarker, with the most highly mutated tumors trending toward improved ICI response rates, but the correlation is not robust (15, 16). Additionally, collecting and analyzing patient samples to evaluate tumor mutational burden can be invasive, expensive, and is not always feasible.

The development of methods to measure immune activity during ongoing therapy also remains a significant challenge. Peripheral immune analyses are currently non-standardized, typically require either knowledge of the antigen(s) of interest or access to adequate tumor tissue to provide said antigen(s), and the results of these assays may not accurately reflect the immune status within the tumor microenvironment (TME). Traditional imaging technologies, such as positron emission tomography (PET) and computed tomography (CT), are utilized to measure tumor volume, but the tumor volume alone may be deceiving if the immunotherapy is driving an influx of beneficial tumor-reactive immune cells. This phenomenon, known as pseudoprogression, mimics tumor growth, but is typically followed by at least a partial response to therapy (17). Given the need for better monitoring options, there has been considerable activity in the development of more relevant immune imaging technologies. The most common PET imaging modality for oncology uses an <sup>18</sup>F-radiolabeled glucose analog (FDG), which detects metabolically active tumors.

Since active immune cells will also take up FDG, it is difficult to distinguish tumor versus immune cell FDG uptake after immunotherapy (18). A small study evaluated whether FDG PET imaging could provide an early prediction of therapeutic response 12–18 weeks after initiation of ICI (19). The authors observed a “flare” defined as >100% standardized uptake value (SUV) increase from baseline without a corresponding increase in tumor volume in 2/7 patients with subsequent complete tumor regression, but an absence of this flare was not predictive of outcomes. More recently, efforts have turned to the development of novel imaging agents designed to specifically measure immune cell presence and/or activity within the tumor, including tracers targeting CD3, CD4, CD8, IL-12, IL-2R, granzyme B, inducible co-stimulator (ICOS), and the immunoPET tracer we have developed against interferon gamma (IFN $\gamma$ ) (20–26).

Initially discovered as an anti-viral cytokine, IFN $\gamma$  also plays a critical role in the interaction between cancer and the immune system (27, 28). IFN $\gamma$  is secreted primarily by innate NK and NKT cells, and adaptive Th1-skewed CD4 and cytotoxic CD8 T cells, and IFN $\gamma$  is a necessary component of an efficacious anti-tumor immune response (29). The clinical importance of IFN $\gamma$  as an inflammatory mediator is evident; an anti-IFN $\gamma$  antibody (Emapalumab) has been FDA approved for treating hemophagocytic lymphohistiocytosis, which is driven by IFN $\gamma$  signaling (30). We have developed an immunoPET tracer utilizing a radiolabeled antibody to IFN $\gamma$  to monitor response to cancer immunotherapy, and we previously demonstrated that anti-IFN $\gamma$  PET can identify HER2 cancer vaccine-induced intratumoral immune activation (26). In the current study, we further validated the utility of our IFN $\gamma$  immunoPET tracer to detect anti-tumor immunity *in situ* using a pre-clinical model that is responsive to ICI. We then evaluated the downstream effect of the tracer antibody on IFN $\gamma$  signaling by measuring expression of interferon regulatory factor 1 (IRF1) (31). Finally, we tested whether the tracer dose of anti-IFN $\gamma$  antibody inhibits ICI efficacy.

## Materials and methods

### Mice and cell lines

BALB/c-syngeneic CT26 colorectal cancer cells, a tumor that is characterized as having a high mutational burden without microsatellite instability (32), were directly purchased from ATCC (CRL-2638) and maintained for fewer than 5 passages. All *in vivo* experiments were performed on 6–8 week old BALB/c mice (The Jackson Laboratory, strain #:000651) after a minimum of 48 hours acclimatization, and all procedures were performed in accordance with guidelines and regulations set by the Wayne State University Institutional Animal Care and Use Committee. Inoculations were given subcutaneously on the right inguinal quadrant with  $2 \times 10^5$  CT26 cells suspended in sterile RPMI (Gibco, 72400047). Tumor growth was monitored by caliper measurement 3 times per week and tumor volume was calculated as  $(W \times W \times L)/2$ .

## Treatment with ICI

Mice were randomly distributed into treated and untreated groups. ICI was given by intraperitoneal injection with 200 µg anti PD-1 (clone RMP1-14, P362, Leinco Technologies) and 100 µg anti CTLA-4 (clone 9D9, C2855, Leinco Technologies) in 200 µL sterile saline.

## Radiochemistry and PET imaging

Radiochemistry of anti-mouse-IFN $\gamma$  (clone AN18, Thermo Fisher Scientific) and IgG1 isotype control anti-horseradish peroxidase (clone HRPN, BE0088, BioXCell) was performed as described previously (22, 26). All antibodies were conjugated to p-SCN-Bn-Desferrioxamine (DFO) with a 1:5 mole ratio of mAb : DFO in saline at pH ~9 for 1hr at 37°C. Unbound DFO was removed via spin column centrifugation (MWCO: 30 kDa, GE Vivaspin 500).  $^{89}\text{Zr}$  (3D Imaging) was incubated with the mAb-DFO conjugates at pH ~ 7.2-7.4 at room temperature for 1hr. Unbound  $^{89}\text{Zr}$  was removed via spin column centrifugation (MWCO: 30 kDa, GE Vivaspin 500) using saline as eluent buffer. [ $^{89}\text{Zr}$ ]Zr-DFO-anti-IFN $\gamma$  and [ $^{89}\text{Zr}$ ]Zr-DFO-IgG were each labeled at a specific activity of ~5 mCi/mg. Radiochemical yields of both constructs were >95% as determined via radio-instant thin layer chromatography (iTLC, Eckert & Ziegler). Tumor-bearing animals used for imaging were injected i.v. with radiolabeled antibodies ( $189 \pm 31$  µCi) in ~150 µL sterile saline. PET images were acquired 72 hrs post-injection on a Bruker Albira SI microPET/CT system. Images were decay corrected and analyzed in PMOD version 4.304. Volume of Interest (VOI) measurements within tumors were used to determine the uptake of the radiotracer, which is expressed as the maximum injected dose per mL (%ID/mL).

## Quantitative reverse transcribed PCR

Tumor tissue collected from mice was snap-frozen in liquid nitrogen and allowed to decay for >10 half-lives stored at -80°C. Tissue was then homogenized with a Tissue Tearor in TRIzol and RNA was extracted as described by the manufacturer (Thermo Fisher Scientific). cDNA was synthesized using a ProtoScript First Strand cDNA synthesis kit (New England Biolabs) using PolyDT primers. qRT-PCR was conducted with TaqMan probes (Thermo Fisher Scientific) for glyceraldehyde 3-phosphate dehydrogenase (GAPDH) (Mm99999915\_g1), IFN $\gamma$  (Mm01168134\_m1), and IRF1 (Mm01288580\_m1). 10 ng of cDNA/well was used and mRNA quantity was calculated as  $2^{-\Delta\text{CT}}$  relative to GAPDH. Transcripts that failed to amplify in all technical replicates were set to a CT value of 55. Transcripts in which only 1/3 of technical replicates amplified were removed.

## Data and statistical analysis

All imaging analysis was performed in PMOD (version 4.304). Statistical analysis utilized R (version 4.1.2) or GraphPad Prism (version 9.5.1). For all two-way ANOVA comparisons, a test of equal variance among groups was performed. If groups had unequal variance, a general least squares model was used to compare variable effects and to test whether variables interacted. A p-value < 0.05 is considered statistically significant. Statistical comparisons between groups were performed as stated in the figure legends.

## Results

### [ $^{89}\text{Zr}$ ]Zr-DFO-anti-IFN $\gamma$ PET tracer shows specific uptake in tumors treated with ICI

To determine if an anti-IFN $\gamma$  immunoPET tracer could identify intratumoral immune activity after ICI, we utilized BALB/c mice bearing subcutaneous CT26 colorectal cancer as a responsive model for combined ICI (anti-CTLA4 and anti-PD-1) therapy. Mice were inoculated with CT26 on day 0 and treated on days 5 and 8 with combined ICI. On day 8, mice were also given ~200 µCi [ $^{89}\text{Zr}$ ]Zr-DFO-anti-IFN $\gamma$  or an IgG isotype control ([ $^{89}\text{Zr}$ ]Zr-DFO-anti-horseradish peroxidase) tracer, with PET imaging 72 hrs post-injection (Figure 1A) to allow for unbound tracer clearance and optimal imaging per our previous experience (26). At the time of tracer administration there was no significant difference in tumor volume between any of the experimental groups (Figure 1B, left panel); however, at the time of imaging on day 11 post-inoculation, tumor volumes were significantly lower in mice receiving ICI treatment ( $p < 0.0001$  for IFN $\gamma$ ,  $p = 0.0018$  for IgG, Figure 1B, right panel). Importantly, within the treatment groups there was no difference in tumor volume attributable to the IFN $\gamma$  versus the isotype control tracer (Supplementary Figure 1).

Quantitation of tumor tracer uptake illustrated a significant increase in IFN $\gamma$  tracer accumulation in tumors from ICI-treated ( $25.23 \pm 6.48$  %ID/mL) versus untreated mice ( $16.22 \pm 2.68$  %ID/mL,  $p < 0.00055$ , Figures 1C, D). Comparatively, mice receiving the isotype control exhibit a marginal but insignificant difference in tumor tracer uptake between untreated ( $8.49 \pm 1.98$  %ID/mL) versus treated ( $12.06 \pm 5.77$  %ID/mL,  $p = 0.394$ ) animals (Figures 1C, D). Interestingly, there is also a significant difference in uptake between untreated ( $8.49 \pm 1.98$  %ID/mL) mice receiving the IgG isotype versus [ $^{89}\text{Zr}$ ]Zr-DFO-anti-IFN $\gamma$  tracer ( $16.22 \pm 2.68$  %ID/mL,  $p < 0.0001$ ), which suggests baseline IFN $\gamma$  expression may be present in untreated CT26 tumors. This observation is consistent with previous reports indicating CT26 is an immunogenic tumor model with moderate levels of IFN $\gamma$  transcript in the TME (33–35). Consistent with our prior experience, non-specific antibody tracer accumulation is also evident in the liver, which is the primary organ for excretion. Biodistribution studies with this tracer have been performed previously (26).

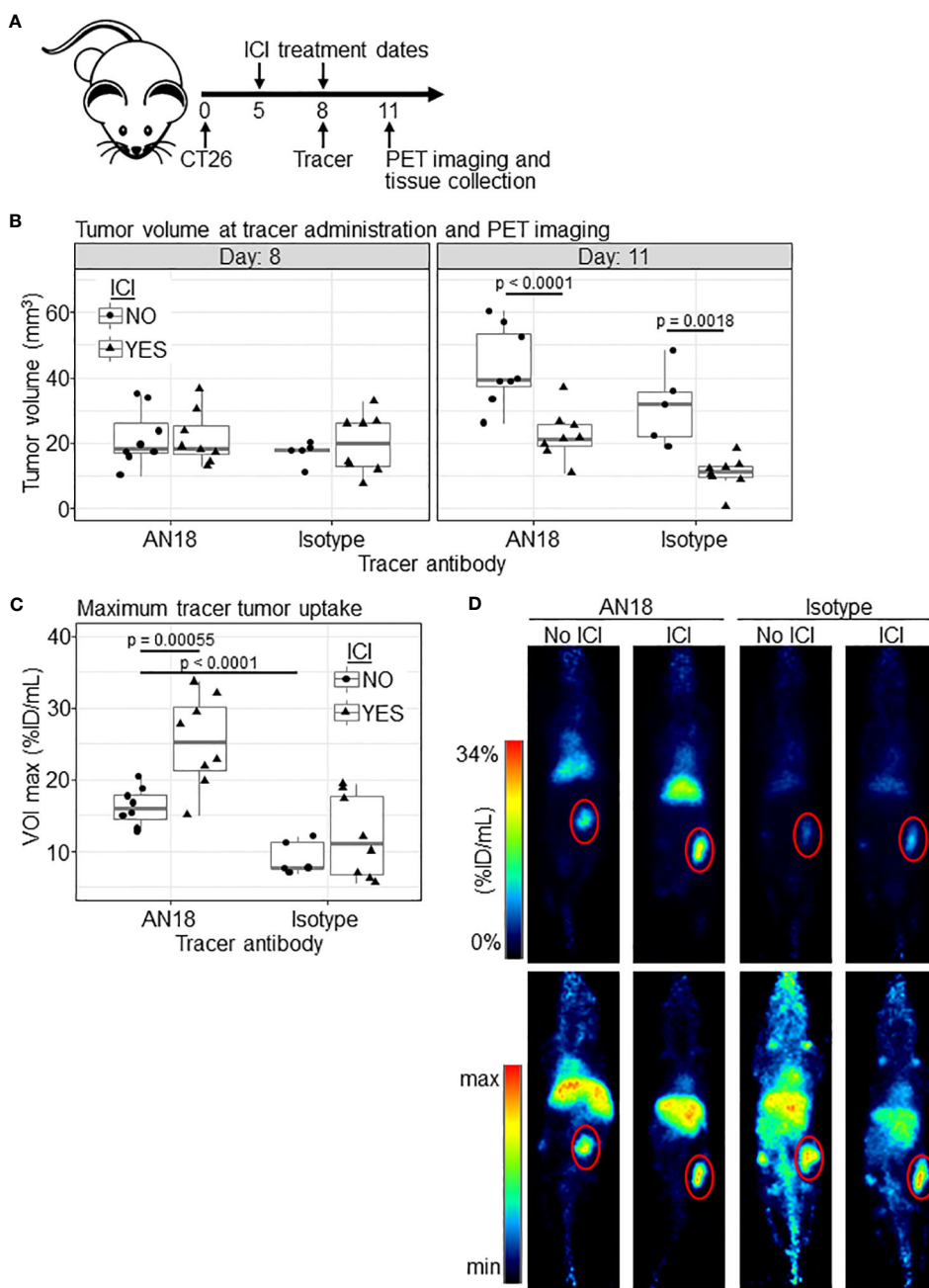


**FIGURE 1**  
<sup>[89Zr]</sup>Zr-DFO-anti-IFN $\gamma$  shows tumor-specific uptake in ICI-treated mice. (A) Schematic of the experiment. (B) CT26 tumor volumes for experimental groups (ICI NO, anti-IFN $\gamma$  tracer n=8; ICI YES, anti-IFN $\gamma$  tracer n=8; ICI NO, isotype control tracer n=5; ICI YES, isotype control tracer n=8) at both tracer injection (day 8, left panel) and PET imaging (day 11, right panel) timepoints. (C) Maximum PET tracer uptake VOI within the tumor in %ID/mL. (D) Representative PET images from animals closest to the mean %ID/mL for the group in (C), with the tumor outlined in red. 2D coronal (top panel) and 3D maximum intensity projection (MIP) (bottom panel) are shown. Significance was determined via Tukey's test after general least squares testing using an interaction model of tracer target and ICI.

### <sup>[89Zr]</sup>Zr-DFO-anti-IFN $\gamma$ PET tracer uptake correlates with ICI treatment outcomes

We next tested whether tumor <sup>[89Zr]</sup>Zr-anti-IFN $\gamma$  uptake would correlate with ICI outcomes. ICI-treated or control CT26-bearing BALB/c mice received ~200  $\mu$ Ci <sup>[89Zr]</sup>Zr-DFO-anti-IFN $\gamma$ , PET imaging was conducted, and tumor volumes were monitored until they reached an experimental endpoint of  $\geq 100$  mm<sup>3</sup> (Figure 2A).

Unlike our initial experiment, at the time of imaging the tumor volume remained similar between treated and untreated groups (Figure 2B); however, we did observe a significant difference in tracer uptake ( $p = 0.018$ , Figures 2C, D). These results suggest that tracer accumulation is independent of tumor volume. Response to ICI is evident, as only 1/8 treated mice failed to eliminate the tumor (Figure 2E). To determine whether tumor tracer uptake correlated to the magnitude of ICI response, we calculated the area under the curve (AUC) of tumor

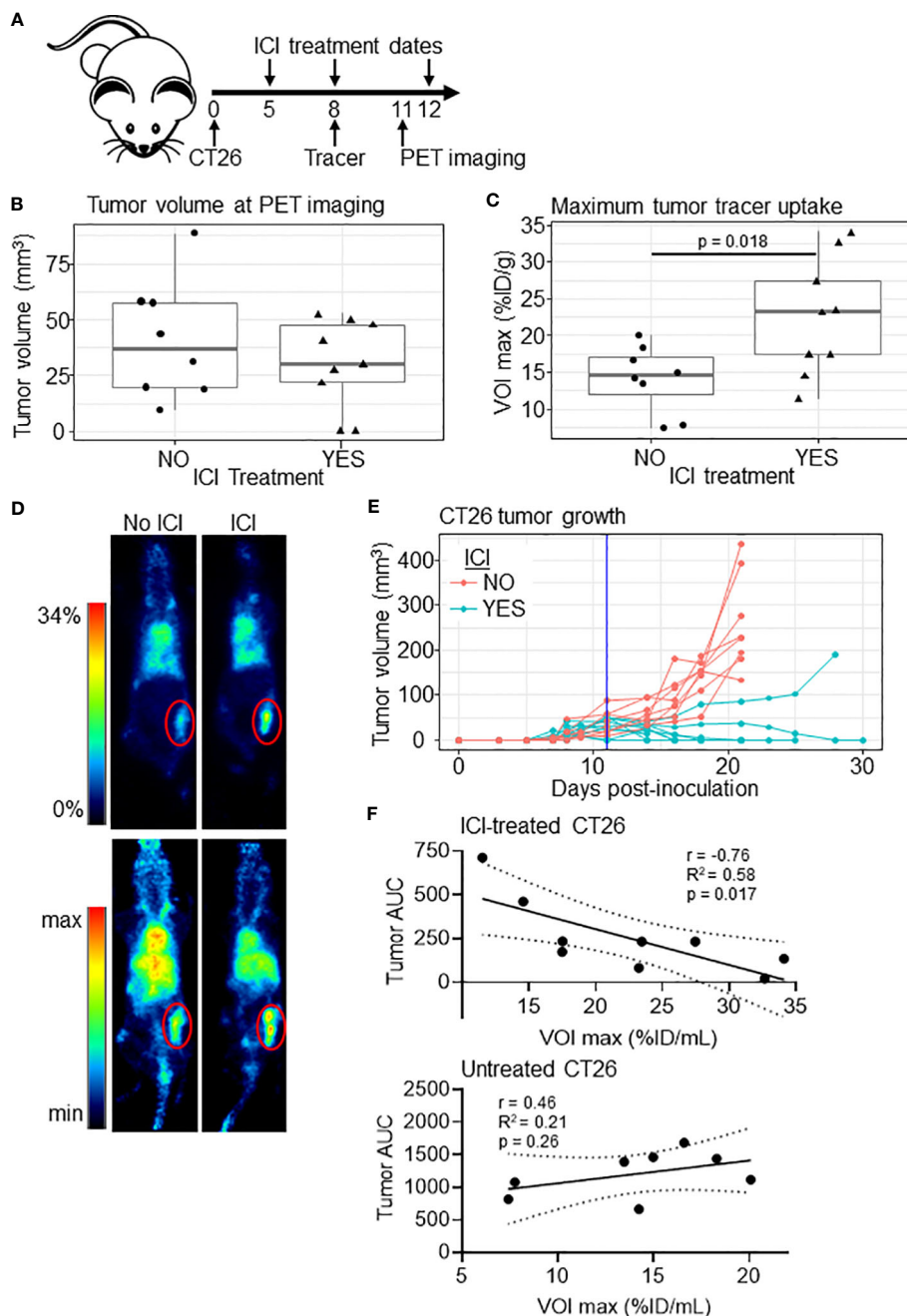


FIGURE 2

$[^{89}\text{Zr}]\text{Zr-DFO-anti-IFN}\gamma$  tumor uptake correlates to tumor burden in treated mice. (A) Schematic of the experiment. (B) Tumor volume of untreated ( $n=8$ ) and ICI-treated ( $n=9$ ) mice at the PET imaging timepoint (day 11). (C) Maximum tumor uptake of  $[^{89}\text{Zr}]\text{Zr-DFO-anti-IFN}\gamma$  tracer VOI in %ID/mL for ICI-treated and untreated mice. Significance determined by Student's T-test. (D) Representative PET images from animals closest to the mean %ID/mL for the group in (C), with the tumor outlined in red. 2D coronal (top panel) and 3D MIP (bottom panel) are shown. (E) Tumor growth in mice bearing CT26 tumors with a vertical line indicating the PET imaging date. (F) Plot of tumor  $[^{89}\text{Zr}]\text{Zr-DFO-anti-IFN}\gamma$  uptake relative to tumor burden measured by area under the curve (AUC) through day 21 for ICI-treated (top panel) and untreated (bottom panel) mice. The Pearson correlation coefficient ( $r$ ), the coefficient of determination ( $R^2$ ), and  $p$  values are shown. Linear correlation is indicated with a solid black line, with a dashed line representing the 95% confidence interval.

volumes for each animal through day 21, at which point all untreated tumors had surpassed our experimental threshold and were euthanized. Within ICI-treated mice, we observed an inverse linear correlation of tumor burden AUC and tracer uptake within the tumor

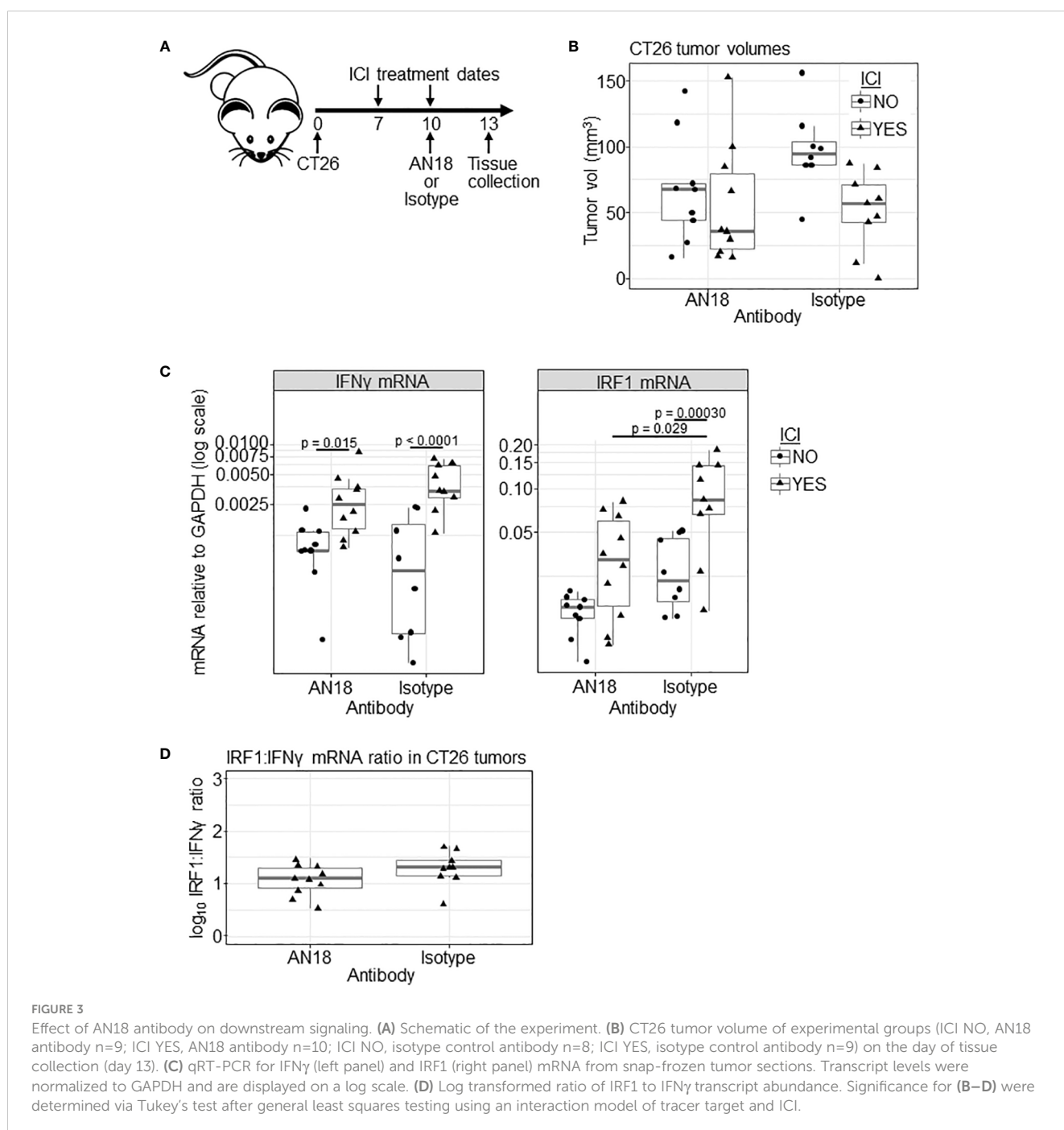
( $r = -0.76$ ,  $R^2 = 0.58$ ,  $p = 0.017$ , Figure 2F, upper panel). Comparatively, in untreated mice there was no significant association between these conditions ( $r = 0.46$ ,  $R^2 = 0.21$ ,  $p = 0.26$ , Figure 2F, lower panel), suggesting tracer uptake is indicative of ICI efficacy.

## The impact of the anti-IFN $\gamma$ antibody tracer on downstream signaling

Because most anti-IFN $\gamma$  antibodies including clone AN18 are neutralizing, we next tested whether the tracer dose of antibody has a detrimental effect on IFN $\gamma$  signaling. Unfortunately, ICI treatment on days 5 and 8 yielded inadequate residual tumor tissue within the treated cohort to extract quality RNA for downstream analysis of IFN $\gamma$  expression and downstream signaling. To give the tumor more time to develop, we shifted the experimental timeline by two days, initiating ICI treatment on day 7, giving tracer antibody (without PET imaging) on day 10, and harvesting tissue

on day 13 (Figure 3A). Upon tissue harvest, we observed no significant differences in tumor volumes between experimental groups (Figure 3B).

We performed qRT-PCR on mRNA extracted from snap-frozen tumor tissue, measuring transcripts for IFN $\gamma$ , to indicate response to ICI, and interferon regulatory factor 1 (IRF1), to indicate whether downstream IFN $\gamma$  signaling is disrupted. Upon IFN $\gamma$  engagement with its receptor, the signal transducer and activator of transcription 1 (STAT1) protein is phosphorylated, translocates the nucleus, and initiates IRF1 mRNA expression (31). Compared to untreated controls, ICI treatment led to increased IFN $\gamma$  mRNA for both AN18 and IgG control antibody-treated groups ( $p = 0.015$  and



$p < 0.0001$ , respectively, Figure 3C). IRF1 transcript, however, was only significantly increased in mice receiving isotype control antibody ( $p = 0.00030$ ), which might suggest that downstream signaling was affected by AN18. In fact, IRF1 expression is higher in ICI-treated mice receiving the control antibody compared to ICI-treated mice receiving AN18 ( $p = 0.029$ ). While IFN $\gamma$  expression itself was not significantly different between these groups, there was a slight elevation of IFN $\gamma$  transcript in mice receiving the control antibody. As an additional test to determine whether the AN18 antibody was impacting IFN $\gamma$  signaling within the tumor, we compared the ratio of IRF1:IFN $\gamma$  transcripts, since IRF1 expression is in part dependent on the presence of IFN $\gamma$  (Figure 3D). There was no significant difference in the ratio of IRF1:IFN $\gamma$  mRNA in ICI-treated mice receiving AN18 or IgG control tracer antibody ( $p = 0.24$ ), suggesting downstream signaling was only marginally affected by AN18, if at all. Collectively these results warranted further evaluation of the impact that the anti-IFN $\gamma$  tracer antibody has on ICI therapeutic efficacy.

### An imaging dose of anti-IFN $\gamma$ antibody does not interfere with ICI response rates

Due to our results from the qRT-PCR analysis, it was important to determine whether the use of an antibody-based IFN $\gamma$  tracer could have a deleterious effect on ICI outcomes. Prior work has demonstrated that AN18 has a neutralizing effect in inflammatory conditions at a single 250  $\mu\text{g}$  dose (36, 37). To investigate whether the tracer dose impacts ICI outcomes, we followed CT26 tumor growth in ICI-treated BALB/c mice receiving 0  $\mu\text{g}$ , 50  $\mu\text{g}$  (the imaging dose), or 250  $\mu\text{g}$  (a neutralizing dose) of cold anti-IFN $\gamma$  antibody with a treatment scheme matching our imaging experiments (Figure 4A). Mice receiving either 0 or 50  $\mu\text{g}$  of anti-IFN $\gamma$  had similar tumor growth curves with 5 of 8 mice eliminating tumor in each group (Figures 4B, C). ICI-treated mice receiving 250  $\mu\text{g}$  AN18 tended to succumb to tumor, with only 1 of 8 mice achieving complete tumor regression. Survival analysis for ICI-treated mice across AN18 doses shows borderline significance between groups receiving 0  $\mu\text{g}$  versus 250  $\mu\text{g}$  ( $p = 0.041$ ) and 50

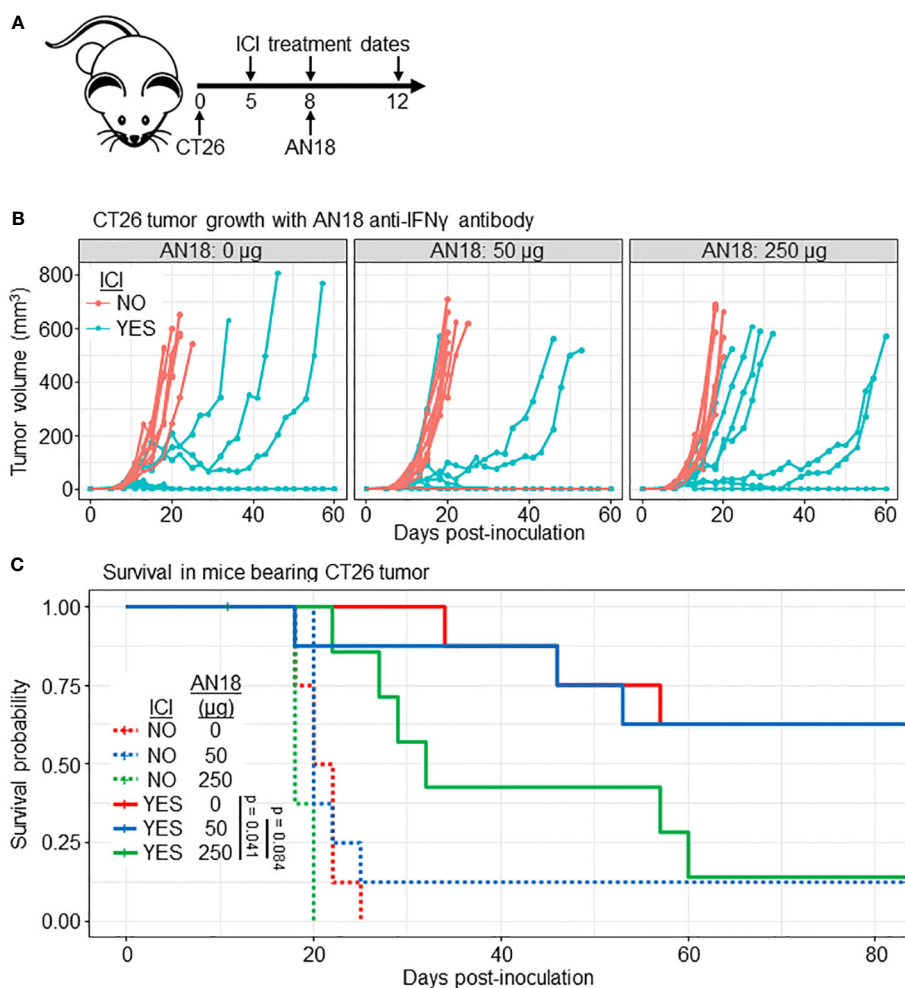


**FIGURE 4** Imaging dose of AN18 antibody does not impact ICI efficacy. (A) Schematic of the experiment. (B) CT26 tumor volume of experimental groups ( $n=8$  per group). (C) Kaplan-Meier survival plot from mice in (B) to depict survival differences among treated mice receiving different dose of anti-IFN $\gamma$  antibody. Significance is determined by Log-rank (Mantel-Cox) test.

$\mu\text{g}$  versus 250  $\mu\text{g}$  ( $p = 0.084$ ) AN18. Importantly, there was no difference between survival of ICI-treated mice receiving 0  $\mu\text{g}$  versus 50  $\mu\text{g}$  AN18 ( $p = 0.95$ ). This data suggests that while neutralization of IFN $\gamma$  impedes ICI efficacy, the imaging dose of anti-IFN $\gamma$  does not negatively impact therapeutic outcomes in this model.

## Discussion

Clinical monitoring of response to ICI remains difficult due in part to pseudoprogression and hyperprogression, both of which can be observed with traditional imaging during immunotherapy treatment (38, 39). This is partly resolved by the more recent iRECIST classification to determine progression, but better methods to predict and monitor response to ICI are still needed (40). The results of this study support the use of a PET tracer to the soluble cytokine IFN $\gamma$  as a promising candidate for immunotherapy evaluation. We found that tumor-localized [ $^{89}\text{Zr}$ ]Zr-DFO-anti-IFN $\gamma$  tracer uptake correlated with ICI treatment outcomes in CT26 tumor-bearing mice. Importantly, in most cases the elevated tracer uptake values preceded a treatment-induced reduction in tumor volumes, highlighting the potential for this tracer to identify intratumoral immune activity within the early stages of treatment.

We utilized an irrelevant IgG antibody to validate the specificity of the anti-IFN $\gamma$  tracer, and while we observed that ICI treatment did not significantly increase control tracer uptake, we did see variability in the amount of tracer detected within tumors from this group (Figure 1C). This finding could be due to increased vascular permeability during an active immune response, which has been associated with expression of IFN $\gamma$  and other cytokines (41). It has been shown that enhanced permeability and retention (EPR) can increase the concentration of macromolecules including IgG; however, there is little known regarding the effect of ICI on tumor vasculature and/or EPR, and it remains unclear whether these changes correlate with ICI response (42, 43). The variable uptake of the isotope control tracer after ICI may be an indicator of treatment-induced alterations within the TME that non-specifically contribute to antibody accumulation.

Our analysis of downstream signaling suggested that the tracer dose may have a physiologic effect, and thus we tested whether this was sufficient to hinder ICI outcomes. A cold anti-IFN $\gamma$  tracer-dose of AN18 antibody did not have a negative effect on ICI therapeutic outcome, while a 5-fold higher, neutralizing dose dampened efficacy. IFN $\gamma$  has a complex paradoxical relationship with both pro- and anti-tumor effects (28, 44–48). Recent studies have shown IFN $\gamma$  has a profound effect on tumor signaling and can act as an inducer of ICI resistance (49–51). A mechanistic study in the B16 melanoma model demonstrated that IFN $\gamma$ -driven resistance mechanisms may be due to signaling effects on tumor cells, and disruption of tumor-specific IFN $\gamma$  signaling can rescue ICI sensitivity (49). It is possible that a sub-neutralizing dose of anti-IFN $\gamma$  might dampen the pro-tumor effects of IFN $\gamma$  signaling while preserving anti-tumor immunity.

Of note, anti-IFN $\gamma$  tracer uptake was elevated compared to an isotope control tracer in untreated mice (Figures 1C, D). The CT26

tumor model is known to be immunogenic and responsive to immunotherapy (33–35), and our results suggest that anti-IFN $\gamma$  PET may be able to detect localized pre-treatment IFN $\gamma$  expression. This raises the question as to whether anti-IFN $\gamma$  PET could be used to detect underlying immune activity, in turn identifying patients with historically non-responsive malignancies who may benefit from immunotherapy.

Previous studies have indicated that response to immunotherapy is dependent on characteristics of both the mouse strain and the specific tumor line (33, 35). We chose to utilize CT26-bearing BALB/c mice because of their responsiveness to ICI, but it will be important to expand upon our findings to include additional models. Our treatment scheme did not produce a 100% response rate, and thus we were able to correlate tracer uptake to tumor burden (Figure 2F). Importantly, tracer administration and/or imaging occurred prior to significant changes in volume between treated and untreated mice in most experiments, supporting their predictive value. However, future studies with less-responsive models would allow for a deeper investigation of whether the tracer can truly predict therapeutic outcomes in less ideal circumstances.

We found that tracer accumulation within the tumor correlated to tumor burden in our efficacy study (Figure 2); however, it is important to note that treatment was initiated 5 days after inoculation, and tumor burden was relatively low at the time of imaging ( $30.3 \pm 19.8 \text{ mm}^3$ ). Slower-growing tumor models, where treatment can be delayed until tumors are larger, may have more clinical relevance and provide more insight into the correlation of tumor burden to tumor tracer uptake. It will be important to determine whether IFN $\gamma$  PET can identify intratumoral immune activity in patients treated with ICI, and whether tumor location or size influences imaging efficacy. It is anticipated that the liver would remain the primary route of excretion for a full-length antibody tracer (52), which may confound efforts to image primary hepatocellular carcinoma, or liver metastases derived from other tumor sites. Injection of excess unlabeled cold antibody immediately prior to tracer may ameliorate this effect (53); however in the case of IFN $\gamma$  antibody, a 5X antibody dose suppressed ICI therapeutic efficacy (Figures 4B, C). Another possible alternative is the use of antibody fragments in place of full-length antibody. Liver accumulation may be reduced, however accumulation is often detected in other organs, including the kidneys (52). In addition to these considerations, an important first step to clinical translation will be the selection of a suitable anti-human IFN $\gamma$  antibody clone, as AN18 does not cross-react with the human protein.

The immune landscape of cancer is complicated and biomarker discovery for immunotherapy has been full of promise, but definitive, dependable biomarkers have yet to be defined (54). Broad classifications of the cancer immune landscape cluster within, but also span across multiple cancer types (55). Consistent signatures of an ICI-responsive immune phenotype may also extend to historically less-responsive malignancies. Reliable, non-invasive biomarkers could help bolster clinical implementation of immunotherapy, and imaging modalities that capture immune activity within the tumor may serve an important role in

monitoring and predicting therapeutic response. The findings of this study demonstrate the potential to meet this need with immunoPET tracers targeting IFN $\gamma$ .

## Data availability statement

The original contributions presented in the study are included in the article/Supplementary Material. Further inquiries can be directed to the corresponding author.

## Ethics statement

The animal study was approved by Wayne State University Institutional Animal Care and Use Committee. The study was conducted in accordance with the local legislation and institutional requirements.

## Author contributions

JH: Formal Analysis, Investigation, Methodology, Validation, Writing – original draft, Writing – review & editing. NR: Methodology, Writing – review & editing. SB: Methodology, Writing – review & editing. MB: Methodology, Writing – review & editing. NV: Conceptualization, Writing – review & editing, Funding acquisition. HG: Conceptualization, Formal Analysis, Funding acquisition, Investigation, Methodology, Project administration, Supervision, Writing – original draft, Writing – review & editing.

## Funding

The author(s) declare financial support was received for the research, authorship, and/or publication of this article. Research was funded in part by the National Cancer Institute under NIH. Award numbers include R37 CA220482 (HG and NV), and the Ruth L. Kirschstein National Research Service Award T32-CA009531 (JH). Research funding was also provided by the Lilly Research Award Program (LRAP) (HG and NV). The authors acknowledge the Microscopy, Imaging, and Cytometry Resources

## References

- Waterhouse P, Penninger JM, Timms E, Wakeham A, Shahinian A, Lee KP, et al. Lymphoproliferative disorders with early lethality in mice deficient in *ctla-4*. *Science* (1995) 270(5238):985–8. doi: 10.1126/science.270.5238.985
- Tivol EA, Borriello F, Schweitzer AN, Lynch WP, Bluestone JA, Sharpe AH. Loss of CTLA-4 leads to massive lymphoproliferation and fatal multiorgan tissue destruction, revealing a critical negative regulatory role of CTLA-4. *Immunity* (1995) 3(5):541–7. doi: 10.1016/1074-7613(95)90125-6
- Nishimura H, Nose M, Hiai H, Minato N, Honjo T. Development of lupus-like autoimmune diseases by disruption of the PD-1 gene encoding an ITIM motif-carrying immunoreceptor. *Immunity* (1999) 11(2):141–51. doi: 10.1016/S1074-7613(00)80089-8
- Wherry EJ. T cell exhaustion. *Nat Immunol* (2011) 12(6):492–9. doi: 10.1038/ni.2035

Core (MICR), which is supported in part by the National Institutes of Health (NIH) Cancer Center Support Grant P30 CA022453 to the Karmanos Cancer Institute at Wayne State University.

## Acknowledgments

We thank Maria Muñiz for reviewing this manuscript and providing insight and suggestions. We also would like to thank the WSU Grid Team for their help in utilizing the High-Performance Computing Grid. We also thank the WSU Division of Animal Laboratory Resources (DLAR) for their care and oversight of the animals in this study.

## Conflict of interest

HG and NV are inventors on US 11,672,877-B2 “In vivo immunoimaging of interferon-gamma.”

The remaining authors declare that the research was conducted in the absence of any commercial or financial relationships that could be construed as a potential conflict of interest.

## Publisher's note

All claims expressed in this article are solely those of the authors and do not necessarily represent those of their affiliated organizations, or those of the publisher, the editors and the reviewers. Any product that may be evaluated in this article, or claim that may be made by its manufacturer, is not guaranteed or endorsed by the publisher.

## Supplementary material

The Supplementary Material for this article can be found online at: <https://www.frontiersin.org/articles/10.3389/fonc.2023.1285117/full#supplementary-material>

### SUPPLEMENTARY FIGURE 1

Plot of tumor volume grouped by treatment and tracer. Lines connect group means. Parallel lines indicate no interaction between treatment and tracer.

- Tawbi HA, Schadendorf D, Lipson EJ, Ascierto PA, Matamala L, Castillo Gutiérrez E, et al. Relatlimab and nivolumab versus nivolumab in untreated advanced melanoma. *N Engl J Med* (2022) 386(1):24–34. doi: 10.1056/NEJMoa2109970
- Marin-Acevedo JA, Kimbrough EMO, Lou Y. Next generation of immune checkpoint inhibitors and beyond. *J Hematol Oncol* (2021) 14(1):1–29. doi: 10.1186/s13045-021-01056-8
- Hellmann MD, Rizvi NA, Goldman JW, Gettinger SN, Borghaei H, Brahmer JR, et al. Nivolumab plus ipilimumab as first-line treatment for advanced non-small-cell lung cancer (CheckMate 012): results of an open-label, phase 1, multicohort study. *Lancet Oncol* (2017) 18(1):31–41. doi: 10.1016/S1470-2045(16)30624-6
- Motzer RJ, Tannir NM, McDermott DF, Arén Frontera O, Melichar B, Choueiri TK, et al. Nivolumab plus ipilimumab versus sunitinib in Advanced Renal-Cell Carcinoma. *N Engl J Med* (2018) 378(14):1277–90. doi: 10.1056/NEJMoa1712126

9. Hellmann MD, Paz-Ares L, Bernabe Caro R, Zurawski B, Kim S-W, Carcereny Costa E, et al. Nivolumab plus ipilimumab in advanced non-small-cell lung cancer. *N Engl J Med* (2019) 381(21):2020–31. doi: 10.1056/NEJMoa1910231
10. Hellmann MD, Ciuleanu T-E, Pluzanski A, Lee JS, Otterson GA, Audigier-Valette C, et al. Nivolumab plus ipilimumab in lung cancer with a high tumor mutational burden. *N Engl J Med* (2018) 378(22):2093–104. doi: 10.1056/NEJMoa1801946
11. Wolchok JD, Kluger H, Callahan MK, Postow MA, Rizvi NA, Lesokhin AM, et al. Nivolumab plus ipilimumab in advanced melanoma. *N Engl J Med* (2013) 369(2):122–33. doi: 10.1056/NEJMoa1302369
12. Larkin J, Chiarion-Sileni V, Gonzalez R, Grob J-J, Rutkowski P, Lao CD, et al. Five-year survival with combined nivolumab and ipilimumab in advanced melanoma. *N Engl J Med* (2019) 381(16):1535–46. doi: 10.1056/NEJMoa1910836
13. Wolchok JD, Chiarion-Sileni V, Gonzalez R, Rutkowski P, Grob J-J, Cowey CL, et al. Overall survival with combined nivolumab and ipilimumab in advanced melanoma. *N Engl J Med* (2017) 377(14):1345. doi: 10.1056/NEJMoa1709684
14. Teng F, Meng X, Kong L, Yu J. Progress and challenges of predictive biomarkers of anti PD-1/PD-L1 immunotherapy: A systematic review. *Cancer Lett* (2018) 414:166–73. doi: 10.1016/j.canlet.2017.11.014
15. Cristescu R, Mogg R, Ayers M, Albright A, Murphy E, Yearley J, et al. Pan-tumor genomic biomarkers for PD-1 checkpoint blockade-based immunotherapy. *Science* (2018) 362(6411):eaar3593. doi: 10.1126/science.aar3593
16. Yarchoan M, Hopkins A, Jaffe EM. Tumor mutational burden and response rate to PD-1 inhibition. *N Engl J Med* (2017) 377(25):2500–1. doi: 10.1056/NEJMcl1713444
17. Chiou VL, Burotto M. Pseudoprogression and immune-related response in solid tumors. *J Clin Oncol* (2015) 33(31):3541. doi: 10.1200/JCO.2015.61.6870
18. Aide N, Hicks RJ, Le Tourneau C, Lheureux S, Fanti S, Lopci E. FDG PET/CT for assessing tumour response to immunotherapy: Report on the EANM symposium on immune modulation and recent review of the literature. *Eur J Nucl Med Mol Imaging* (2019) 46(1):238–50. doi: 10.1007/s00259-018-4171-4
19. Chang B, Huang A, Shang C, Palmer K, Schubert E, Xu W, et al. Evaluation of the anti-PD-1 flare response in patients with advanced melanoma using FDG PET/CT imaging and hematologic biomarkers. *J Nucl Med* (2019) 60(supplement 1).
20. Larimer BM, Wehrenberg-Klee E, Caraballo A, Mahmood U. Quantitative CD3 PET imaging predicts tumor growth response to anti-CTLA-4 therapy. *J Nucl Med* (2016) 57(10):1607–11. doi: 10.2967/jnumed.116.173930
21. Kristensen LK, Fröhlich C, Christensen C, Melander MC, Poulsen TT, Galler GR, et al. CD4+ and CD8+ PET imaging predicts response to novel PD-1 checkpoint inhibitor: studies of Sym021 in syngeneic mouse cancer models. *Theranostics* (2019) 9(26):8221–38. doi: 10.7150/tno.37513
22. Viola NT, Glassbrook JE, Kalluri JR, Hackett JB, Wicker MN, Sternberg J, et al. Evaluation of an immunoPET tracer for IL-12 in a preclinical model of inflammatory immune responses. *Front Immunol* (2022) 13. doi: 10.3389/fimmu.2022.870110
23. van de Donk PP, Wind TT, Hooiveld-Noeken JS, van der Veen EL, Glaudemans AWJM, Diepstra A, et al. Interleukin-2 PET imaging in patients with metastatic melanoma before and during immune checkpoint inhibitor therapy. *Eur J Nucl Med Mol Imaging* (2021) 48(13):4369–76. doi: 10.1007/s00259-021-05407-y
24. Larimer BM, Wehrenberg-Klee E, Dubois F, Mehta A, Kalomeris T, Flaherty K, et al. Granzyme B PET imaging as a predictive biomarker of immunotherapy response. *Cancer Res* (2017) 77(9):2318–27. doi: 10.1158/0008-5472.CAN-16-3346
25. Xiao Z, Mayer AT, Nobashi TW, Gambhir SS. ICOS is an indicator of T-cell-mediated response to cancer immunotherapy. *Cancer Res* (2020) 80(14):3023–32. doi: 10.1158/0008-5472.CAN-19-3265
26. Gibson HM, McKnight BN, Malysa A, Dyson G, Wiesend WN, McCarthy CE, et al. Interferon- $\gamma$  PET imaging as a predictive tool for monitoring response to tumor immunotherapy. *Cancer Res* (2018) 78(19):5706. doi: 10.1158/0008-5472.CAN-18-0253
27. Milstone LM, Waksman BH. Release of virus inhibitor from tuberculin-sensitized peritoneal cells stimulated by antigen. *J Immunol* (1970) 105(5):1068–71. doi: 10.4049/jimmunol.105.5.1068
28. Castro F, Cardoso AP, Gonçalves RM, Serre K, Oliveira MJ. Interferon-gamma at the crossroads of tumor immune surveillance or evasion. *Front Immunol* (2018) 9(MAY):337231. doi: 10.3389/fimmu.2018.00847
29. Fallarino F, Gajewski TF. Cutting edge: differentiation of antitumor CTL *in vivo* requires host expression of stat1. *J Immunol* (1999) 163(8):4109–13. doi: 10.4049/jimmunol.163.8.4109
30. Al-Salama ZT. Emapalumab: first global approval. *Drugs* (2019) 79(1):99–103. doi: 10.1007/s40265-018-1046-8
31. Ivashkiv LB. IFN $\gamma$ : signalling, epigenetics and roles in immunity, metabolism, disease and cancer immunotherapy. *Nat Rev Immunol* (2018) 18(9):545–58. doi: 10.1038/s41577-018-0029-z
32. Castle JC, Loewer M, Boegel S, de Graaf J, Bender C, Tadmor AD, et al. Immunomic, genomic and transcriptomic characterization of CT26 colorectal carcinoma. *BMC Genomics* (2014) 15(1):190. doi: 10.1186/1471-2164-15-190
33. Lechner MG, Karimi SS, Barry-Holson K, Angell TE, Murphy KA, Church CH, et al. Immunogenicity of murine solid tumor models as a defining feature of *in vivo* behavior and response to immunotherapy. *J Immunother* (2013) 36(9):477–89. doi: 10.1097/01.cji.0000436722.46675.4a
34. Beatty GL, Paterson Y. IFN-gamma can promote tumor evasion of the immune system *in vivo* by down-regulating cellular levels of an endogenous tumor antigen. *J Immunol* (2000) 165(10):5502–8. doi: 10.4049/jimmunol.165.10.5502
35. Yu JW, Bhattacharya S, Yanamandra N, Kilian D, Shi H, Yadavilli S, et al. Tumor-immune profiling of murine syngeneic tumor models as a framework to guide mechanistic studies and predict therapy response in distinct tumor microenvironments. *PLoS One* (2018) 13(11):e0206223. doi: 10.1371/journal.pone.0206223
36. Sawitzki B, Kingsley CI, Oliveira V, Karim M, Herber M, Wood KJ. IFN- $\gamma$  production by alloantigen-reactive regulatory T cells is important for their regulatory function *in vivo*. *J Exp Med* (2005) 201(12):1925. doi: 10.1084/jem.20050419
37. Sacchi A, Gasparri A, Curnis F, Bellone M, Corti A. Crucial role for interferon gamma in the synergism between tumor vasculature-targeted tumor necrosis factor alpha (NGR-TNF) and doxorubicin. *Cancer Res* (2004) 64(19):7150–5. doi: 10.1158/0008-5472.CAN-04-1445
38. Chae YK, Wang S, Nimeiri H, Kalyan A, Giles FJ. Pseudoprogression in microsatellite instability-high colorectal cancer during treatment with combination T cell mediated immunotherapy: a case report and literature review. *Oncotarget* (2017) 8(34):57889–97. doi: 10.18632/oncotarget.18361
39. Costa LB, Queiroz MA, Barbosa FG, Nunes RF, Zaniboni EC, Ruiz MM, et al. Reassessing patterns of response to immunotherapy with PET: from morphology to metabolism. *Radiographics* (2021) 41(1):120–43. doi: 10.1148/rg.2021200093
40. Seymour L, Bogaerts J, Perrone A, Ford R, Schwartz LH, Mandrekas S, et al. iRECIST: guidelines for response criteria for use in trials testing immunotherapeutics. *Lancet Oncol* (2017) 18(3):e143. doi: 10.1016/S1470-2045(17)30074-8
41. Martin S, Maruta K, Burkart V, Gillis S, Kolb H. IL-1 and IFN-gamma increase vascular permeability. *Immunology* (1988) 64(2):301.
42. Matsumura Y. Barriers to antibody therapy in solid tumors, and their solutions. *Cancer Sci* (2021) 112(8):2939–47. doi: 10.1111/cas.14983
43. Matsumura Y, Maeda H. A New Concept for Macromolecular Therapeutics in Cancer Chemotherapy: Mechanism of Tumor-tropic Accumulation of Proteins and the Antitumor Agent Smanes1 (2023). Available at: [http://aacrjournals.org/cancerres/article-pdf/46/12\\_Part\\_1/6387/2424185/cr04612p16387.pdf](http://aacrjournals.org/cancerres/article-pdf/46/12_Part_1/6387/2424185/cr04612p16387.pdf).
44. MR Z, Zaidi MR. The interferon-gamma paradox in cancer. *J Interferon Cytokine Res* (2019) 39(1):30–8. doi: 10.1089/jir.2018.0087
45. Takeda K, Nakayama M, Hayakawa Y, Kojima Y, Ikeda H, Imai N, et al. IFN- $\gamma$  is required for cytotoxic T cell-dependent cancer genome immunoeediting. *Nat Commun* (2017) 8:14607. doi: 10.1038/ncomms14607
46. Dunn GP, Ikeda H, Bruce AT, Koebel C, Uppaluri R, Bui J, et al. Interferon-gamma and cancer immunoeediting. *Immunol Res* (2005) 32(1–3):231–45. doi: 10.1385/IR.32.1-3:231
47. Ni L, Lu J LN, J L. Interferon gamma in cancer immunotherapy. *Cancer Med* (2018) 7(9):4509–16. doi: 10.1002/cam4.1700
48. Alspach E, Lussier DM, Schreiber RD. Interferon  $\gamma$  and its important roles in promoting and inhibiting spontaneous and therapeutic cancer immunity. *Cold Spring Harb Perspect Biol* (2019) 11(3):a028480. doi: 10.1101/cshperspect.a028480
49. Benci JL, Johnson LR, Choa R, Xu Y, Qiu J, Zhou Z, et al. Opposing functions of interferon coordinate adaptive and innate immune responses to cancer immune checkpoint blockade. *Cell* (2019) 178(4):933–948.e14. doi: 10.1016/j.cell.2019.07.019
50. Benci JL, Xu B, Qiu Y, Wu TJ, Dada H, Twyman-Saint Victor C, et al. Tumor interferon signaling regulates a multigenic resistance program to immune checkpoint blockade. *Cell* (2016) 167(6):1540–1554.e12. doi: 10.1016/j.cell.2016.11.022
51. Thibaut R, Bost P, Milo I, Cazaux M, Lemaître F, Garcia Z, et al. Bystander IFN- $\gamma$  activity promotes widespread and sustained cytokine signaling altering the tumor microenvironment. *Nat Cancer* (2020) 1(3):302–14. doi: 10.1038/s43018-020-0038-2
52. Manafi-Farid R, Ataeinia B, Ranjbar S, Jamshidi Araghi Z, Moradi MM, Pirich C, et al. ImmunoPET: antibody-based PET imaging in solid tumors. *Front Med* (2022) 9. doi: 10.3389/fmed.2022.916693
53. Mortimer JE, Bading JR, Colcher DM, Conti PS, Frankel PH, Carroll MI, et al. Functional imaging of human epidermal growth factor receptor 2-positive metastatic breast cancer using (64)Cu-DOTA-trastuzumab PET. *J Nucl Med* (2014) 55(1):23–9. doi: 10.2967/jnumed.113.122630
54. Arora S, Velichinskii R, Lesh RW, Ali U, Kubiak M, Bansal P, et al. Existing and emerging biomarkers for immune checkpoint immunotherapy in solid tumors. *Adv Ther* (2019) 36(10):2638–78. doi: 10.1007/s12325-019-01051-z
55. Thorsson V, Gibbs DL, Brown SD, Wolf D, Bortone DS, Ou Yang TH, et al. The immune landscape of cancer. *Immunity* (2018) 48(4):812–830.e14. doi: 10.1016/j.immuni.2018.03.023